

Enhancing hydrogen evolution reaction using iridium atomic monolayer on conventional electrodes: A first-principles study

Abdul Ahad Mamun, Asif Billah, Muhammad Anisuzzaman Talukder*

Department of Electrical and Electronic Engineering, Bangladesh University of Engineering and Technology, Dhaka 1205, Bangladesh

ARTICLE INFO

Keywords:

Solar hydrogen generation
Electrochemical cell
Electrolysis
Electrodes

ABSTRACT

In a water-electrolysis system for hydrogen production, the kinetics of hydrogen evolution reaction (HER) critically depend on the exchange current density (J_0) of the electrode. Noble metals, e.g., Pt, Ir, Rh, and Au, offer a significant J_0 when used as electrodes, assisting faster HER. However, instead of using expensive noble metals as electrodes, a thin layer on conventional electrodes, e.g., Ni, Cu, Ag, and Mo, also increases J_0 . An electrode's J_0 during HER is calculated from the free energy of hydrogen adsorption (ΔG_H), which is determined from hydrogen adsorption energy (E_{ad}) on the electrode surface. This work considered an Ir atomic monolayer as an electrocatalyst on the (111) plane of conventional Ni, Cu, Ag, and Mo electrodes, producing modified Ir/Ni(111), Ir/Cu(111), Ir/Ag(111), and Ir/Mo(111) electrodes. This work calculated E_{ad} of the modified electrodes using the density functional theory (DFT). In addition, this work develops an advanced kinetic model for the exchange current density considering the concentration of hydrogen ions (C_{H^+}) and partial pressure of hydrogen gas (P_{H_2}). The dependence of activation overpotential (η_a) vs. J_0 relationship on C_{H^+} and P_{H_2} in HER is investigated. For the modified electrodes, J_0 increases by 10^2 – 10^3 times compared to the conventional electrodes, resulting in efficient H_2 production with low losses.

1. Introduction

The worldwide energy demand is growing tremendously with the rapidly increasing population, a significant concern nowadays due to the limitations of fossil fuels, such as scarcity, emission of greenhouse gases, and negative impacts on the environment [1]. Hydrogen (H_2) is a better alternative to fossil fuels to meet the energy demand [2–4]. H_2 is a promising energy source that meets zero carbon emissions and has no adverse environmental impact during operation, as the byproducts are simply heat and water. [5–7]. The dynamic range of global H_2 demand is rising rapidly, with estimates from 73 to 158 Mt by 2030, 300 Mt by 2040, and 568 Mt by 2050, based on the present scenario [8]. H_2 can be produced by electrocatalytic or photoelectrocatalytic water splitting in an electrochemical cell (EC) or a photoelectrochemical cell (PEC), respectively, through a cathodic hydrogen evolution reaction (HER). In HER, protons (H^+) from an electrolytic solution react with electrons at the electrode surface to produce chemically adsorbed hydrogen atoms (H^*), eventually producing H_2 . Here, the electrode is crucial in adsorbing H^* and charge transfer kinetics with the electrolytic solution.

During the past decade, there has been renewed interest in HER dynamics, and researchers are exploring low-cost alternatives to noble metal-based electrodes [3,4,6]. Du et al. developed a unique datura-shaped electrode using Ni-HG-rGO-Ni, incorporating Ni nanoparticles,

hydrophilic graphene (HG), and reduced graphene oxide (rGO) layers on Ni foam, and the developed electrode exhibited effective charge transfer efficiency and good HER performance in alkaline solution [9]. (N, P) co-doped in Ni metal electrode had been developed by a multifaceted heteroatom-doping method, exhibiting higher HER activity with lower overpotential and good electronic structure similar to noble metal-like catalytic properties [10]. Transition metal-based alloy NiFeMo electrode designed by Hsieh et al. exhibited good HER and OER activities in basic media with a cell voltage of 1.47 V and a current density of 10 mAcm^{-2} for overall water splitting, outperforming the Pt/C and IrO_2 catalytic properties [11]. High charge kinetic activities, durability, and stability of electrodes are crucial in PECs for efficient H_2 generation. Recently, several electrocatalysts have been reported to enhance HER [5,7,12–16].

Transition metal carbides (TMCs), transition metal phosphides (TMP), transition metal chalcogenides (sulfides and selenides), and carbon-based electrocatalysts have received extensive attention in the development of non-noble metal-based electrocatalysts to achieve desirable catalytic activity and stability in both acid and basic solutions [17,18]. Notably, noble metal-based electrocatalysts exhibit outstanding electrocatalytic activity during HER due to their ranks at the top of the volcano curve [19,20]. The electron work function,

* Corresponding author.

E-mail address: anis@eee.buet.ac.bd (M.A. Talukder).

<https://doi.org/10.1016/j.ijhydene.2024.02.156>

Received 24 October 2023; Received in revised form 5 February 2024; Accepted 11 February 2024

Available online 13 February 2024

0360-3199/© 2024 Hydrogen Energy Publications LLC. Published by Elsevier Ltd. All rights reserved.

crystal structure, Pauling electronegativities, and the free energy for H_2 adsorption (ΔG_H) of electrode materials primarily determine the HER electrocatalytic activity [21–28]. The rate of charge transfer kinetics in equilibrium is defined as the exchange current density (J_0). Hence, J_0 represents the rate of H evolution per surface area at the electrode and is typically used to evaluate an electrode's capacity to catalyze the HER. In practice, the electron exchange rate during HER between the electrode and the electrolytic solution is calculated using the kinetic model proposed by Nørskov et al. that relates J_0 , rate constant (k_0), and ΔG_H [21,29]. A greater J_0 results in a faster HER and minimizes the associated losses, e.g., activation overpotential (η_a), hydrogen crossover, and ohmic losses [30].

Electrode materials have variable J_0 . The earth-abundant and low-cost conventional transition metal electrodes, e.g., Ni, Cu, Ag, and Mo, have a small J_0 due to their large ΔG_H [21,31]. Conventional electrodes also suffer from low electrical conductivity in HER, a limited number of exposed active sites, sacrificial oxidation on surfaces, and relatively unstable and high overpotential, significantly limiting their catalytic performances for HER [32–35]. Platinum, a noble metal, and other Pt-group materials, e.g., Ir, Rh, and Au, are most suitable for HER. Unfortunately, Pt-group noble metals' low natural abundance and high expenses limit their massive deployment for H_2 generation. Therefore, the design and fabrication of electrocatalysts on conventional electrodes for HER by utilizing minimum noble metal usage are in urgent demand. Various electrocatalysts have been developed to realize this goal in recent years [34,36]. Zhang et al. developed a noble metal (Ag, Au, Cu, Pd, and Pt)-doped MoS_2 electrode, which exhibited excellent performance in HER by reducing the activation energy of water splitting [37]. The smaller amount of Pt nanoparticles deposited on carbon-based materials enhanced adsorption active sites and electrical conductivity, which allows fast charge transfer during HER kinetics [38,39]. An atomic monolayer of a noble metal grown on conventional electrodes can be an excellent electrocatalyst for HER with high charge transfer kinetics, durability, and stability. Both spontaneously and electrochemically deposited monolayers on conventional electrodes substantially increase the active surface area and can produce a highly HER-active electrode [34,40]. Notably, the monolayer can impose its electronic properties on the overall surface electronic properties [41].

Recently, ΔG_H has been studied for conventional electrodes with noble metal monolayers, e.g., Ru, Pt, Rh, and Au, using the density functional theory (DFT) [42,43]. In earlier works, Madey et al. and Schröder et al. reported electrodes with the deposition of atomically thin two-dimensional (2D) Pt layers on W and Cu substrates, respectively, exhibiting an increase in active surface area and stability [44, 45]. In addition, 2D Rh nanosheets with a thickness of 0.8 nm corresponding to 6 atomic layers deposited on carbon nanotubes (CNTs) had ~20.40-fold enhancement in mass-activity for hydrolysis [46]. It has several remarkable advantages, e.g., high electrocatalytic activity, electrical conductivity, chemical stability, and corrosion resistance compared to the other noble metals [42]. Using a first principles approach, this work investigates utilizing Ir atomic monolayer on the (111) plane of low-cost earth-abundant conventional electrodes, e.g., Ni, Cu, Ag, and Mo, for HER. This work chose the (111) plane as it has a tightly packed arrangement of atoms, forming equilateral triangles with the highest atomic density. Here, conventional electrodes with Ir atomic monolayer are considered modified electrodes, i.e., Ir/Ni(111), Ir/Cu(111), Ir/Ag(111), and Ir/Mo(111) electrodes.

In a PEC, the improvement of electrodes significantly impacts the H_2 generation. We analyze ΔG_H , H adsorption energy (ΔE_{ads}), electrocatalytic activity, and the impact of η_a for HER. ΔG_H and electronic density of states (DOS) of the modified electrodes have been determined using the DFT calculations. The impacts of electrodes' surface coverage by H^* (θ_{sc}) are investigated considering the atop, fcc, and hcp adsorption sites. The obtained ΔG_H values for the modified electrodes are approximately twice smaller than those of the conventional electrodes. This

work develops an advanced kinetic model to predict J_0 considering ambient temperature (T), the concentration of H^+ (C_{H^+}), and the partial pressure of H_2 (P_{H_2}) in the context of practical scenario in a water-splitting system. The calculated J_0 of the modified electrodes is $\sim 10^2$ – 10^3 times greater than conventional electrodes considering $T = 298.15$ K, $C_{H^+} = 0.5$ M, and $P_{H_2} = 1$ atm. The effects of η_a on HER have been investigated by calculating J_0 from the Butler-Volmer equation in PECs. η_a is significantly smaller in the modified electrodes than in conventional electrodes due to improved J_0 .

2. Advanced kinetic model for exchange current density

In HER, H_2 is produced at the cathodic electrode. The total HER reaction can be written as



This reaction takes place in the active sites of the electrode surface. The intermediate reactions are



where the superscript “*” denotes the active site of the electrode surface and H^* denotes the adsorbed hydrogen. The final step of HER and the net current density (J) due to charge transfer between the electrode surface and the electrolytic solution are



$$J = -er. \quad (3b)$$

In Eq. (3), $r = r_f - r_b$ is the net reaction rate of HER, where r_f and r_b are the forward and backward reaction rates, respectively. When the total reaction, as given in Eq. (1), reaches equilibrium, the forward and backward current densities become equal so that $J_0 = J_{f,eq} = J_{b,eq} = -er_0$, where r_0 is the equilibrium reaction rate [31,47,48].

In HER, the electrocatalytic activity at electrodes proportionately depends on J_0 . Nørskov et al. proposed a simple kinetic model for HER on transition electrode surfaces to predict J_0 so that $J_0 = k_0 \times f(\Delta G_H)$, where k_0 is the electrocatalytic rate constant and $f(\Delta G_H)$ is a function of ΔG_H [31]. Nørskov model relates J_0 with k_0 and ΔG_H for adsorption and desorption of hydrogen on electrode surfaces by

$$J_0 = ek_0 \exp(-\Delta G_H/k_B T) C_{tot}(1 - \theta) \quad \text{for } \Delta G_H > 0, \quad (4a)$$

$$J_0 = ek_0 C_{tot}(1 - \theta) \quad \text{for } \Delta G_H < 0, \quad (4b)$$

where C_{tot} , k_B , e , and θ stand for the total adsorption sites per area, Boltzmann constant, electronic charge, and adsorption coverage of H, respectively. The rate constant k_0 is determined from experimental data considering electrolyte concentration, reaction rates of HER, and transfer coefficient of electrons between electrode and electrolyte with the micro-kinetic model [49]. It is assumed that k_0 has a universal rate constant value, which equals $200 \text{ s}^{-1} \text{ site}^{-1}$ for all electrodes [31,50].

J_0 is related to θ for both $\Delta G_H < 0$ and $\Delta G_H > 0$. The findings of the “ab initio thermodynamic study” show that θ reaches its maximum and forms a complete surface coverage when ΔG_H is negative, helping attraction to H [21,51]. On the contrary, θ is minimum when ΔG_H is positive, showing repulsion to H. Langmuir model describes that $\theta = K/(1 + K)$, where $K = \exp(-\Delta G_H/k_B T)$ [21,52]. The above description related to the model leads to [31]

$$J_0 = -ek_0 \frac{\exp(-\Delta G_H/k_B T)}{1 + \exp(-\Delta G_H/k_B T)} C_{tot} \quad \text{for } \Delta G_H > 0, \quad (5a)$$

$$J_0 = -ek_0 \frac{1}{1 + \exp(-\Delta G_H/k_B T)} C_{tot} \quad \text{for } \Delta G_H < 0. \quad (5b)$$

The difference in free energy between H in its gas phase and when it is adsorbed, ΔG_{H} , is calculated by [31]

$$\Delta G_{\text{H}} = \Delta E_{\text{ads}} + \Delta E_{\text{ZPE}} - T\Delta S. \quad (6)$$

The zero-point energy (ZPE), ΔE_{ZPE} , represents the energy of the H molecule when it is in a free or unbound state before it interacts with the electrode surface. The value of ΔE_{ZPE} is typically less than 0.05 eV for all electrodes [31]. Furthermore, ΔS is the entropy difference between H in its gas phase and when it is adsorbed, referring to the change in the degree of disorder of H molecules as they transition from a gas phase to an adsorbed phase on an electrode surface. It is typically included as a correction term for ΔG_{H} . At room temperature, hydrogen's gas phase entropy, $-\frac{1}{2}S_{\text{H}_2}^0$, is ~ 1.35 meV/K [53]. This work considered $\Delta E_{\text{ZPE}} - T\Delta S = 0.24$ eV for all electrodes [21,31]. ΔG_{H} is critically correlated to ΔE_{ads} , which depends on the electrode's material. ΔE_{ads} can be calculated by DFT using the following relationship [21]

$$\Delta E_{\text{ads}} = \frac{1}{n}(E_{\text{slab}/n\text{H}^*} - E_{\text{slab}} - \frac{n}{2}E_{\text{H}_2}), \quad (7)$$

where E_{slab} is the relaxed and optimized electrode surface energy, $E_{\text{slab}/n\text{H}^*}$ is the system energy when adsorbed H^* is placed on the electrode surface, E_{H_2} is the H_2 energy, and n is the total adsorbed H_2 . Considering the above phenomena of ZPE, entropy, and adsorption energy, Eq. (6) becomes [31]

$$\Delta G_{\text{H}} = \Delta E_{\text{ads}} + 0.24 \text{ eV}. \quad (8)$$

Although some disparities exist between the experimental and DFT-computed k_0 values, the difference can be significantly minimized if k_0 is considered electrode-dependent rather than universal, as in the original Norskov model. Timothy and his colleagues created a kinetic model that increases fidelity by incorporating k_0 dependency on electrode [21]. They showed that the kinetic prefactor k_0 depends proportionately on ΔG_{H} . Another reason for the dissimilarity between the experimental and computed J_0 values is not considering C_{H^+} and P_{H_2} .

Theoretical descriptions of a PEC's current density–voltage (J – V) characteristics that depend on P_{H_2} and C_{H^+} are still being developed. It is acknowledged that P_{H_2} and C_{H^+} are significant determinants of HER kinetics [54–57]. The effects of P_{H_2} are significant at larger J due to the faster reaction kinetics of HER. Consequently, P_{H_2} affects J_0 , which increases with the higher P_{H_2} for faster adsorption and desorption of H [55,57]. Furthermore, P_{H_2} affects equilibrium potential in a low pH. However, the impact of P_{H_2} is negligible with high pH values due to a smaller C_{H^+} [58–60]. The Nernst equation can be used to explain the pH dependency for HER kinetics, as given in Section 3 within the supplementary. The relationship suggests that the pH of the electrolytic solution and C_{H^+} affect J_0 .

Therefore, this work developed an advanced kinetic model of J_0 by incorporating $k_0^\alpha \exp(\Delta G_{\text{H}})$ instead of k_0 and by inserting $C_{\text{H}^+}^\beta$ and $P_{\text{H}_2}^\gamma$ in Eq. (5). Now, this equation can be written as

$$J_0 = ek_0^\alpha \exp(\Delta G_{\text{H}}) C_{\text{H}^+}^\beta P_{\text{H}_2}^\gamma \frac{\exp(-\Delta G_{\text{H}}/kT)}{1 + \exp(-\Delta G_{\text{H}}/kT)} C_{\text{tot}} \quad \text{for } \Delta G_{\text{H}} > 0, \quad (9a)$$

$$J_0 = ek_0^\alpha \exp(\Delta G_{\text{H}}) C_{\text{H}^+}^\beta P_{\text{H}_2}^\gamma \frac{1}{1 + \exp(-\Delta G_{\text{H}}/kT)} C_{\text{tot}} \quad \text{for } \Delta G_{\text{H}} < 0, \quad (9b)$$

where α , β , and γ are parameters that are associated with k_0 , P_{H_2} , and C_{H^+} . These parameters are calculated from previous experimental reported data using Eq. (9). A selection of experimental data for J_0 is presented in Table S2 to evaluate the advanced kinetic model.

Fig. 1 shows two curves used to compute J_0 values. Fig. 1(a) shows $\log(J_0/\text{Acm}^{-2})$ vs. ΔG_{H} calculated using Eq. (5). On the other hand, Fig. 1(b) shows $\log(J_0/\text{Acm}^{-2})$ vs. ΔG_{H} calculated using Eq. (9), considering α , $C_{\text{H}^+}^\beta$, and $P_{\text{H}_2}^\gamma$ parameters. Both curves display the correlation between HER's ΔG_{H} and $\log(J_0/\text{Acm}^{-2})$. The range of β used in this work was 0.1–0.3. It was found that β had a minimal effect when

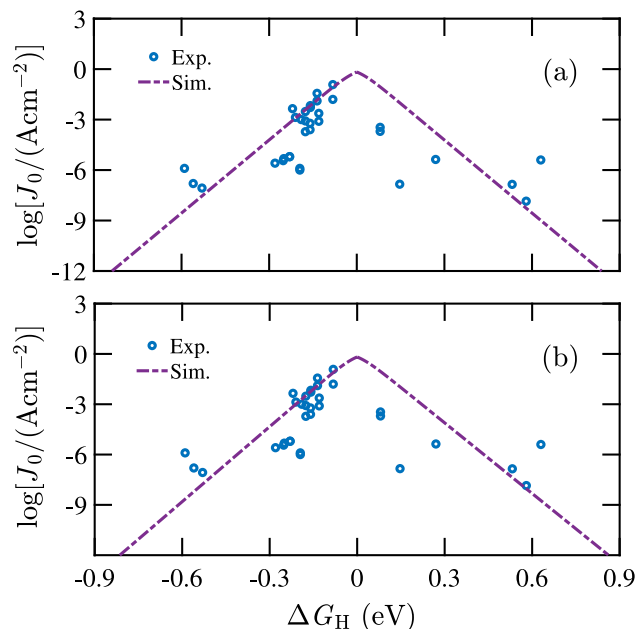


Fig. 1. Correlation between $\log(J_0/\text{Acm}^{-2})$ and ΔG_{H} calculated using (a) Eq. (5), and (b) using Eq. (9) utilizing reported data in Table S2.

$\Delta G_{\text{H}} > 0$ but none at all when $\Delta G_{\text{H}} < 0$. For $\Delta G_{\text{H}} < 0$ and $\Delta G_{\text{H}} > 0$, α values were 1.65 and 1.85, respectively. In addition, γ was found to be 0.4 for both $\Delta G_{\text{H}} < 0$ and $\Delta G_{\text{H}} > 0$, while γ can be measured in the range of 0.3 to 1 experimentally [61].

The absolute error ($\sigma_{\text{e,abs}}$) and standard deviation (σ_{d}) of calculated J_0 in the log scale when compared with experimental values show that the associated equation of Fig. 1(b) is more precise in calculating J_0 . The simulated J_0 values in Fig. 1(a) show $\sigma_{\text{e,abs}} = 1.6264$ and $\sigma_{\text{d}} = 2.2004$, while those of Fig. 1(b) are 1.5691 and 2.1321, respectively. The decreased $\sigma_{\text{e,abs}}$ and σ_{d} of Fig. 1(b) clarify a stronger correlation between the experimental data and the advanced kinetic model. Hence, the equation presented in this work is more accurate at predicting the kinetics of HER and can be utilized to precisely calculate J_0 values under various C_{H^+} and P_{H_2} circumstances. Notably, the empirical parameter, α , allows varying k_0 under $\Delta G_{\text{H}} < 0$ and $\Delta G_{\text{H}} > 0$, supporting the alignment of the electrocatalytic activity with experimental data.

3. Computational methods

This work performs DFT calculations using the self-consistent ab initio method on the Quantum Espresso software [62]. The exchange–correlation energy was determined using the general gradient approximation (GGA) applying Perdew–Burke–Ernzerhof (PBE) functional to generate ultrasoft pseudopotentials [62,63]. Projected augmented wave (PAW) was used to describe the ionic cores, and the valence states were expanded in a basis set of plane waves with a cut-off kinetic energy of 544 eV. The charge density cut-off kinetic energy has been assumed to be twelve times greater than the wavefunction cut-off kinetic energy. The DFT-D3 function was utilized for Van der Waals correction. The Brillouin zone has been sampled by a $7 \times 7 \times 1$ set of k points mesh using the general Monkhorst–Pack scheme [64].

The (1×1) hexagonal supercell geometry was used for modeling electrodes' (111)-plane surfaces with seven atomic layers. An Ir atomic monolayer has been placed on the (111)-plane surfaces. A vacuum of 10 Å was kept above and below the electrode material to avoid the external interaction that occurs for periodicity along the electrode thickness. The H adsorption was allowed on both sides of the electrode

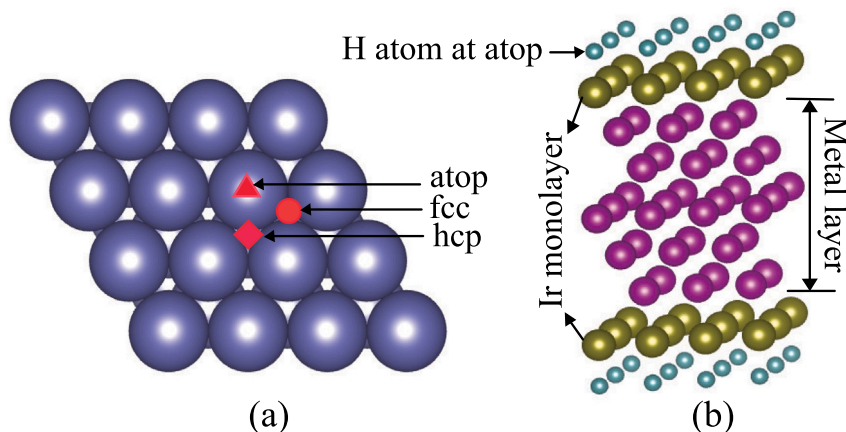


Fig. 2. (a) Different adsorption sites on (111) plane of the electrode. (b) Electrode with Ir atomic monolayer hydrogen adsorption system at atop site.

surface to prevent the periodicity from being electrostatically linked. The geometry of the electrode with Ir monolayer and adsorbed H molecules has been optimized by variable-cell relax calculation with the tolerance of atom-acting forces remaining below 0.05 eV\AA^{-1} . Three specific sites were used to investigate the adsorption: fcc and hcp (three-fold sites) and atop (single-fold site), as shown in Fig. 2(a). The presence of water molecules has a negligible effect on H adsorption and desorption on metal electrode surfaces [65]. Therefore, this work performs calculations without water molecules to analyze the electrocatalytic performances for HER. The complete diagram of the atomic system with Ir atomic monolayer is shown in Fig. 2(b). In this work, $E_{\text{slab}/n\text{H}^*}$, E_{slab} , and E_{H_2} have been computed using the procedure discussed in this section. ΔE_{ads} and ΔG_{H} have been calculated using Eqs. (7) and (8), respectively. J_0 has been determined using the developed advanced kinetic model given in Eq. (9) for HER. Finally, a comprehensive comparison of the conventional and modified electrodes has been investigated based on η_a using the Butler-Volmer equation [66].

4. Result and discussion

4.1. Density of states and hydrogen adsorption energy

In PECs, cathodic electrodes play a key role in producing H_2 . Therefore, studying electrodes' physical and chemical properties is crucial for efficient water splitting. The density of states (DOS) is the number of available electron states per unit volume and energy, determining conductivity. The modified electrodes have good electrical properties, e.g., high electrical conductivity, resistance to corrosion at high temperatures, and no bandgap within the energy band. Fig. 3 shows the DOS of Ir/Ni(111), Ir/Mo(111), Ir/Cu(111), and Ir/Ag(111) electrodes. The d-orbitals are significant in transition metals to describe their degeneracy. Fig. 3 also shows the d-DOS of Ir and the modified electrodes. The modified electrodes show high DOS within a broad energy band due to a larger surface-to-volume ratio than conventional electrodes. Therefore, the modified Ir monolayer-based electrodes will offer high conductivity, enhancing HER significantly [67].

ΔE_{ad} values represent the adhesiveness of an atom to the electrode's surface in different phases, such as gas, liquid, or dissolved solid. In a PEC system, E_{ad} is crucial for the reaction coordinate of H^+ to H_2 by accepting electrons from the electrode surface. The surface has atop, fcc, hcp, and bridge adsorption sites. This work considered only the atop, fcc, and hcp sites for H adsorption. θ_{sc} is defined as the ratio between H^* and the available active sites for H. This work considered $\theta_{\text{sc}} = 1 \text{ ML}$, i.e., fully-covered, and $\theta_{\text{sc}} = 0.5 \text{ ML}$, i.e., half-covered modified electrodes for each site (see Fig. S1).

Table 1
 ΔE_{ad} of conventional electrodes modified by Ir atomic monolayer.

Electrodes	Adsorption Sites	ΔE_{ad} (eV)	
		$\theta_{\text{sc}} = 0.5 \text{ ML}$	$\theta_{\text{sc}} = 1.0 \text{ ML}$
Ir/Ni(111)	atop	-0.131	-0.441
	fcc	0.145	-0.222
	hcp	-0.086	-0.268
Ir/Cu(111)	atop	0.471	-0.251
	fcc	0.325	-0.365
	hcp	0.341	-0.399
Ir/Ag(111)	atop	0.190	-0.268
	fcc	-0.025	-0.528
	hcp	-0.037	-0.550
Ir/Mo(111)	atop	-0.304	-0.561
	fcc	-0.266	-0.255
	hcp	-0.267	-0.280

Table 1 presents the calculated ΔE_{ad} at the atop, fcc, and hcp sites on Ir/Ni(111), Ir/Cu(111), Ir/Ag(111), and Ir/Mo(111) electrodes. The positive ΔE_{ad} indicates that the system energy is higher than the adsorbent energy, i.e., endothermic adsorption. By contrast, negative ΔE_{ad} indicates that the system energy is lower than the adsorbent energy, i.e., exothermic adsorption. The high adsorption energy ($\Delta E_{\text{ad}} \geq |1 \text{ eV}|$) means that the adsorbate is strongly chemically bonded with the adsorbent and H^* does not convert to H_2 gas [68]. The presented ΔE_{ad} values in Table 1 are preferable for HER. The maximum and minimum ΔE_{ad} values are 0.145 eV at the fcc site and -0.131 eV at the atop site, respectively, for Ir/Ni(111) electrode, when $\theta_{\text{sc}} = 0.5 \text{ ML}$. For $\theta_{\text{sc}} = 1.0 \text{ ML}$, the maximum ΔE_{ad} is -0.222 eV at the fcc site, and the minimum ΔE_{ad} is -0.441 eV at the atop site. The maximum ΔE_{ad} is at the atop site for both $\theta_{\text{sc}} = 0.5$ and 1.0 ML for Ir/Cu(111) electrode, but the minimum ΔE_{ad} is found at the fcc site for $\theta_{\text{sc}} = 0.5 \text{ ML}$ and at the hcp site for $\theta_{\text{sc}} = 0.5 \text{ ML}$. For Ir/Ag(111) and Ir/Mo(111) electrodes, the maximum and minimum ΔE_{ad} occurs at the same sites for both $\theta_{\text{sc}} = 0.5$ and 1.0 ML .

The distance of H^* from the electrode surface is shown in Fig. 4 for $\theta_{\text{sc}} = 0.5$ and 1.0 ML . In both cases, the distance of the H-atom at the atop site is approximately the same for each modified electrode. At the fcc and hcp sites, the distance of the H-atom is the same for Ir/Ag(111), Ir/Cu(111), and Ir/Ni(111) electrodes but different in different electrodes. For the Ir/Mo(111) electrode, the distance of H^* is different at the fcc and hcp sites since Mo has a BCC crystal structure, whereas Ag, Cu, and Ni have FCC crystal structures.

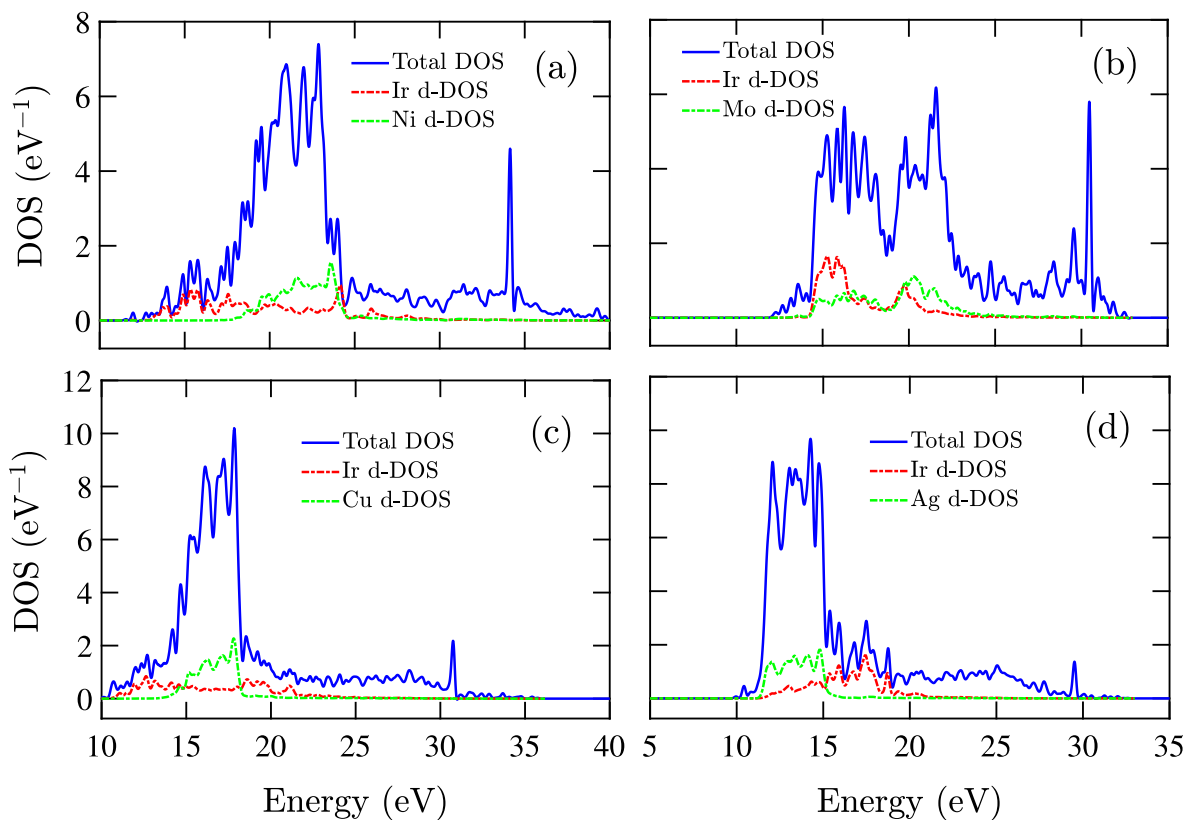


Fig. 3. Electronic properties of (a) Ir/Ni(111) DOS, Ir d-DOS, and Ni d-DOS (b) Ir/Mo(111) DOS, Ir d-DOS, and Mo d-DOS, (c) Ir/Cu(111) DOS, Ir d-DOS, and Ni d-DOS, and (d) Ir/Ag(111) DOS, Ir d-DOS, and Ni d-DOS against electron energy.

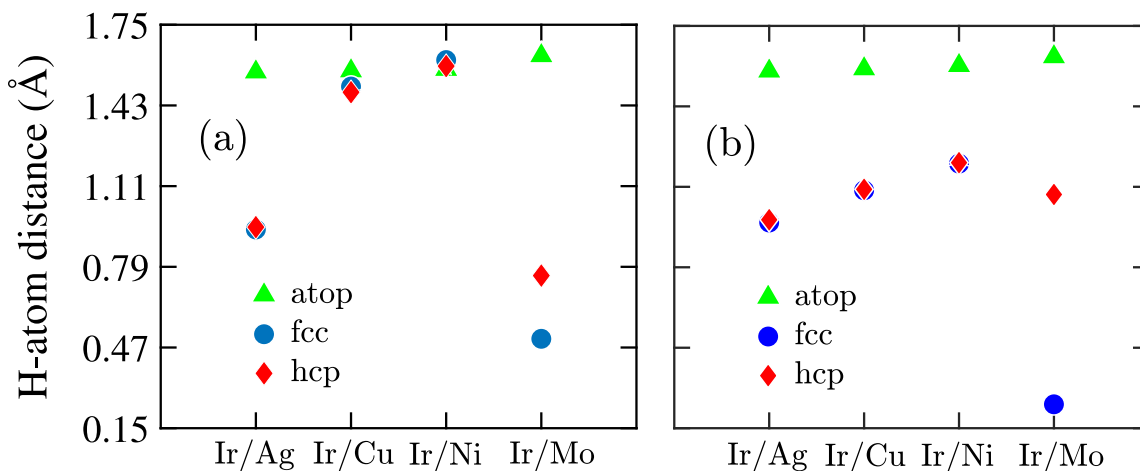


Fig. 4. Distance of H-atom at the atop, fcc, and hcp sites from electrode surface for (a) $\theta_{sc} = 0.5$ ML, and (b) $\theta_{sc} = 1.0$ ML.

4.2. Exchange current density of modified electrodes

J_0 is a crucial parameter governing the HER rate in water splitting. The reaction between H^+ and e^- occurs faster on the electrode surface with a higher J_0 . Therefore, the charge transfer kinetics between the electrode and the electrolytic solution improves if J_0 increases. In this work, J_0 is calculated using Eq. (9) based on ΔG_H of the modified electrodes, k_0 , C_{H^+} , and P_{H_2} parameters. Here, $C_{H^+} = 0.5$ M, $P_{H_2} = 1$ atm, and $T = 298$ K are considered to calculate J_0 . The detailed calculation results of E_{slab/nH^+} , ΔG_H , and J_0 at the atop, fcc, and hcp sites on the modified electrodes are presented in Table S3.

Different sites of the modified electrodes have different values of J_0 . Finding preferable active sites for H adsorption on the electrodes' surface is crucial. The minimum value of E_{slab/nH^+} indicates the site where adsorption and desorption have occurred. H^+ reacts with e^- to produce H_2 gas along a reaction pathway called the reaction coordinate. Fig. 5 illustrates the preferable reaction coordinate for each electrode considering $\theta_{sc} = 0.5$ and 1.0 ML. For $\theta_{sc} = 0.5$ ML, the preferable active site for Ir/Ni(111) electrode is atop, and ΔG_H is 0.101 eV. The preferred active sites are fcc, hcp, and atop for Ir/Cu(111), Ir/Ag(111), and Ir/Mo(111) electrodes, respectively, and the corresponding ΔG_H values are 0.565 eV, 0.203 eV, and -0.064 eV. Here, the Ir/Mo(111) electrode has the lowest activation barrier of reaction, and the Ir/Cu(111) electrode has the highest activation barrier of reaction when considering

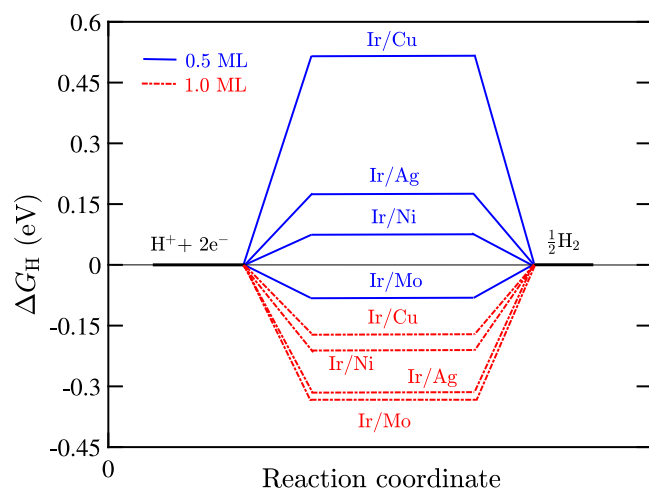


Fig. 5. Reaction coordinate of HER for with Ir atomic monolayer on conventional electrode considering as $\theta_{sc} = 0.5$ and 1.0 ML.

Table 2

Comparison of ΔG_H of the proposed modified electrodes with previously published works with $\theta_{sc} = 1.0$ ML.

Electrode	ΔG_H (eV)	Reference	Electrode	ΔG_H (eV)	Reference
Pd _{ML} /Cu(111)	0.340	[69]	Pt _{ML} /Cu(111)	0.640	[69]
Pt _{SA} /Ni	-0.380	[70]	IrW (alloy)	0.340	[71]
Pd/Au(111)	-0.360	[69]	MoS ₂ /Cu	-0.348	[37]
IrNC (alloy)	0.040	[72]	MoS ₂ /Pd	-0.600	[37]
Ir/Ni(111)	-0.201	This work	Ir/Cu(111)	-0.160	This work
Ir/Ag(111)	-0.310	This work	Ir/Mo(111)	-0.321	This work

$\theta_{sc} = 0.5$ ML. For $\theta_{sc} = 1.0$ ML, the preferable active sites for the modified electrodes are the same as $\theta_{sc} = 0.5$ ML, except for Ir/Cu(111) electrode, which has the preferable active site of hcp. The lowest barrier of ΔG_H is -0.160 eV for Ir/Cu(111) electrode and the highest barrier of ΔG_H is -0.321 eV for Ir/Mo(111) electrode.

The top rank in the volcano curve (J_0 vs. ΔG_H) for an electrode should be required for efficient hydrogen production with low overpotential losses in water-splitting system [19]. The modified electrodes of this work have a better position in the volcano curve, as shown in Fig. 6, and outperform some previously reported data of electrodes with atomic monolayers of different materials, as illustrated in Table 2.

The improved J_0 are $10^{-1.33}$ Acm⁻², $10^{-2.75}$ Acm⁻², and $10^{-1.30}$ Acm⁻² for Ir/Ni(111), Ir/Ag(111), and Ir/Mo(111) electrodes, respectively, when $\theta_{sc} = 0.5$ ML. However, J_0 of Ir/Cu(111) electrode is approximately the same as the conventional Cu electrode due to the larger ΔE_{ad} . The larger ΔE_{ad} indicates a propensity to form chemical bonds, resulting in slow HER rates. On the contrary, at $\theta_{sc} = 1.0$ ML, the improvement of J_0 is significant for Ir/Cu(111). The value of J_0 with $\theta_{sc} = 1.0$ ML decreases for Ir/Ni(111), Ir/Ag(111), and Ir/Mo(111) electrodes but still is higher than those of conventional electrodes. Fig. 6 compares J_0 of the conventional electrodes with the modified electrodes. Fig. 6 also shows an error bar to estimate J_0 with better precision. The error bar represents the variation of the calculated results within $\sigma_d = 2.1321$, determined from Eq. (9) with the experimental data (see Table S2).

4.3. Activation overpotential in modified electrodes

The overpotential is the electrode potential that deviates from the equilibrium potential required for HER. The overpotential arises from the contact impedance between the electrode and solution, the concentration of the solution, and hindrance kinetics in both the cathode and anode [73]. Ideally, water-splitting needs a redox potential of 1.23

V. However, there is a need for an additional 0.4–0.6 V for water electrolysis due to the overpotential losses in a practical scenario [5]. Hence, minimizing the overpotential for efficient hydrogen production is crucial. The total overpotential comprises the activation, ohmic, and concentration overpotentials. The Helmholtz double layer between the electrode and the electrolytic solution in HER causes η_a , which is significant compared to other PEC losses. Notably, J_0 significantly impacts on η_a . The H₂ generation is more effective at a lower η_a , correlated with a higher J_0 [66].

For HER, η_a and J are considered as cathodic overpotential ($\eta_{a,c}$) and cathodic current density J_c , respectively. The Butler-Volmer equation has been used to calculate $\eta_{a,c}$ considering J_0 , C_{H^+} , P_{H_2} , and J_c [66]. This work calculates $\eta_{a,c}$ for the modified electrodes using the resulting J_0 and for the conventional electrode with the experimental J_0 (see Table S2), when $C_{H^+} = 0.5$ M and $P_{H_2} = 1$ atm. Fig. 7 illustrates the $\eta_{a,c}$ vs. J_c for the modified electrodes and for the conventional electrodes with $\theta_{sc} = 0.5$ and 1.0 ML. In this figure, the negative sign of $\eta_{a,c}$ and J_c indicates that the modified electrodes are used as cathodes for HER in PEC. Fig. 7(a–d) also shows that the conventional electrodes have the highest $\eta_{a,c}$, whereas $\eta_{a,c}$ significantly decreases for the modified electrodes, except for the Ir/Cu(111) electrode at $\theta_{sc} = 0.5$ ML due to a higher ΔG_H . In addition, $\eta_{a,c}$ of $\theta_{sc} = 0.5$ ML has the smaller values in comparison with $\eta_{a,c}$ of $\theta_{sc} = 1$ ML, except for the Ir/Cu(111) electrodes.

At $J_c = 100$ mAcm⁻², the highest $\eta_{a,c}$ obtained is 0.455 V, which is for Ir/Mo(111) electrode with $\theta_{sc} = 1$ ML. On the other hand, Ir/Ni(111) and Ir/Ag(111) electrodes show $\eta_{a,c} = 0.255$ V and 0.402 V, respectively. The lowest $\eta_{a,c} = 0.189$ V is found for the Ir/Cu(111) electrode. At $J_c = 1000$ mAcm⁻², $\eta_{a,c} = 0.308$ V with $\theta_{sc} = 1$ ML for the Ir/Cu(111) electrode. Recently, Tan et al. reported $\eta_{a,c} = 0.438$ V for a Pt-deposited Cu electrode, when $J_c = 1000$ mAcm⁻² with $\theta_{sc} = 1$ ML [74]. Hence, this work achieves a significant decrease in $\eta_{a,c}$ for Cu electrodes. Consequently, H₂ can be produced at a smaller applied voltage using the modified electrodes.

Fig. 8 shows the effects of C_{H^+} and P_{H_2} for the Ir/Ni(111) electrode with $\theta_{sc} = 1$ ML. Fig. 8(a) depicts the effects of C_{H^+} on J_c vs. $\eta_{a,c}$ at a constant $P_{H_2} = 1$ atm. At this constant pressure, $C_{H^+} = 0.25$ M has the highest $\eta_{a,c}$, whereas $C_{H^+} = 1.25$ M has the lowest $\eta_{a,c}$. A higher value of C_{H^+} increases J_0 to enhance the reaction kinetics of HER. Consequently, $\eta_{a,c}$ decreases due to the increased J_0 . However, $\eta_{a,c}$ does not vary linearly with C_{H^+} . The decreasing of $\eta_{a,c}$ is significant in the range of $C_{H^+} = 0.25$ to 0.75 M, but eventually, the trends of decreasing becomes less significant when the value of C_{H^+} reaches closer to 1.25 M. Fig. 8(b) shows the effects of P_{H_2} on J_c vs. $\eta_{a,c}$ with $C_{H^+} = 0.5$ M. The maximum and minimum $\eta_{a,c}$ are found at $P_{H_2} = 0.6$ and 1.4 atm, respectively. The changing trend of $\eta_{a,c}$ with P_{H_2} is analogous to the trend of Fig. 8(a) due to the proportional relationship between P_{H_2} and J_0 . Additionally, the increased P_{H_2} helps the withdrawal of hydrogen bubbles from the electrode surface to drive the HER kinetics faster with low losses.

In brief, this work contributes to developing an advanced kinetic model for J_0 and enhancing the electrocatalytic activity of conventional electrodes (e.g., Ni, Cu, Ag, and Mo) in water splitting with an Ir atomic monolayer. The advanced kinetic model accounts for the effects of C_{H^+} and P_{H_2} and precisely predicts J_0 for HER under a practical scenario. The atomic monolayer signifies that only a minute amount of material is required to develop the modified electrode. Compared to the conventional electrodes, the modified electrodes show an excellent rise in J_0 , 10^2 – 10^3 times, reducing η_a and increasing hydrogen production. These contributions are significant to advancing sustainable energy, especially in light of hydrogen gas's potential as a fuel source to meet the world's energy needs.

5. Conclusion

H₂ produced from water-splitting is a promising option for fuel to meet worldwide energy demand. The H₂ production performance

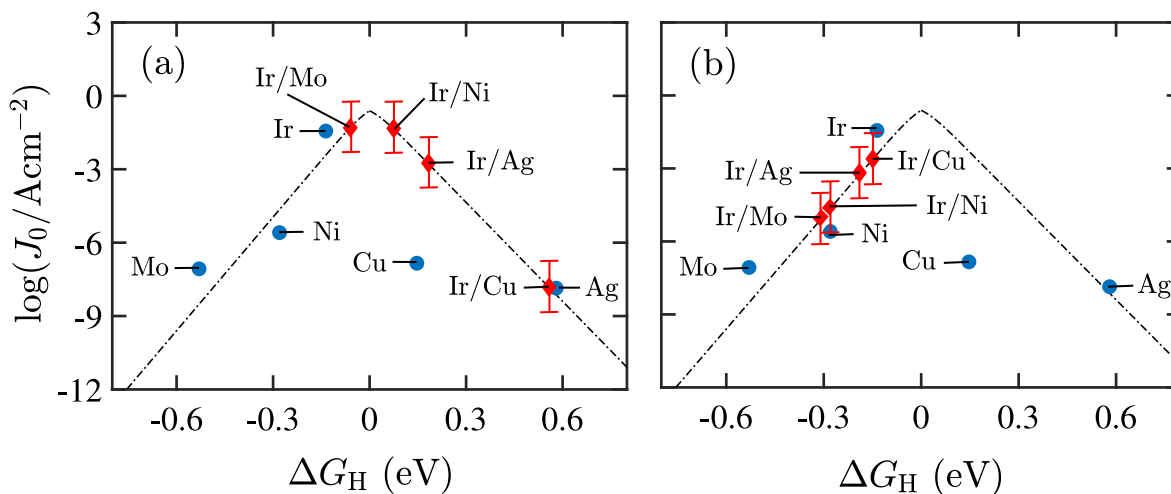


Fig. 6. Comparison of $\log(J_0/A_{cm^{-2}})$ vs. ΔG_H of conventional electrodes (Ni, Cu, Ag, Mo) and Ir atomic monolayer-based modified electrodes with (a) $\theta_{sc} = 0.5$ ML and (b) $\theta_{sc} = 1.0$ ML. The blue circle indicates experimental values for conventional electrodes, and the red line indicates simulation results for modified electrodes.

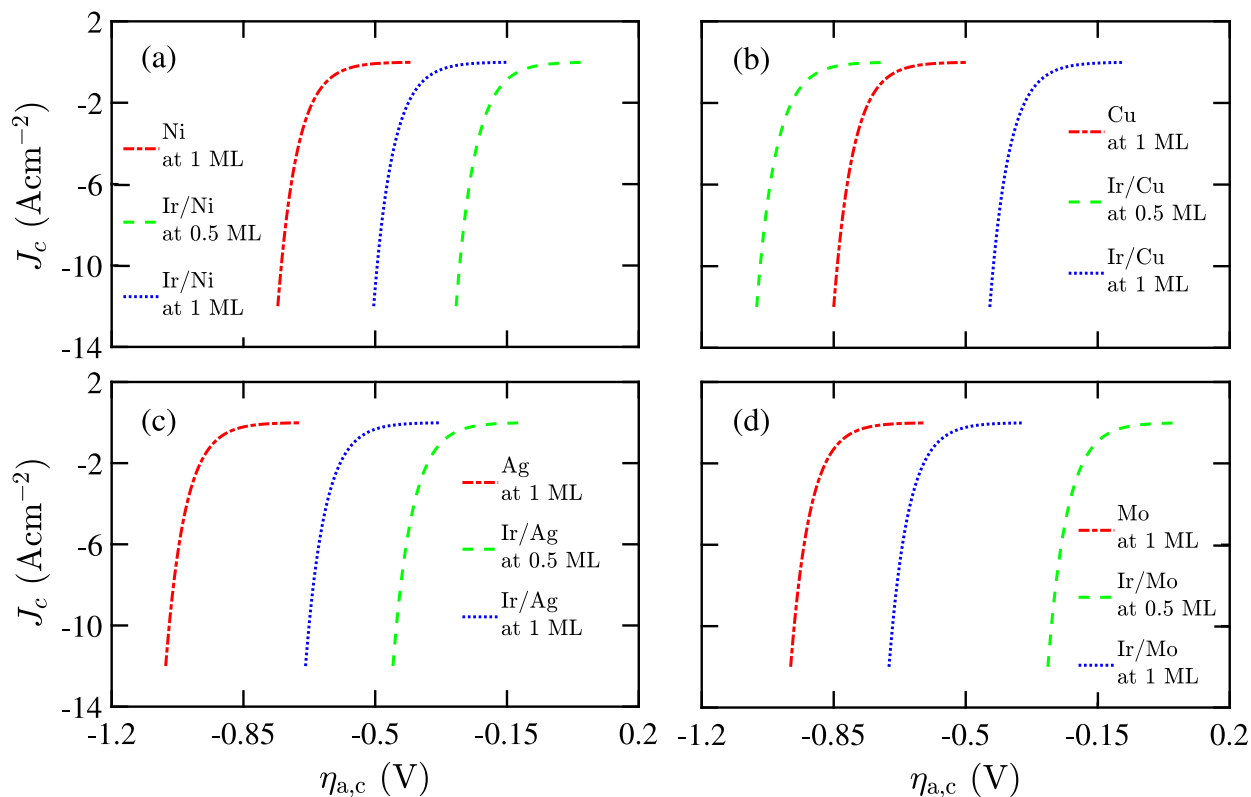


Fig. 7. The impact of J_c vs. $\eta_{a,c}$ with $\theta_{sc} = 0.5$ and 1.0 ML for (a) Ni and Ir/Ni(111), (b) Cu and Ir/Cu(111), (c) Ag and Ir/Ag(111), (d) Mo and Ir/Mo(111).

of an electrochemical water-splitting system critically depends on J_0 of the electrodes. The conventional electrodes have a smaller J_0 and consequently slower HER kinetics. This work considered modified electrodes utilizing an Ir monolayer on conventional electrodes to increase J_0 so that the HER can be faster. This work also developed an advanced kinetic model for J_0 including C_{H^+} and P_{H_2} . For the modified electrodes, J_0 increases by 10^2 – 10^3 times concerning the conventional electrodes. The increased J_0 helps the reaction kinetics of HER occur faster with smaller η_a . The η_a of the modified electrodes decreases twice compared to the conventional electrodes. Therefore, the modified electrodes enhance the reaction kinetics of HER, reduce energy losses, and produce H_2 more effectively for upcoming sustainable energy development worldwide.

Declaration of competing interest

The authors declare that they have no known competing financial interests or personal relationships that could have appeared to influence the work reported in this paper.

Appendix A. Supplementary data

Supplementary material related to this article can be found online at <https://doi.org/10.1016/j.ijhydene.2024.02.156>.

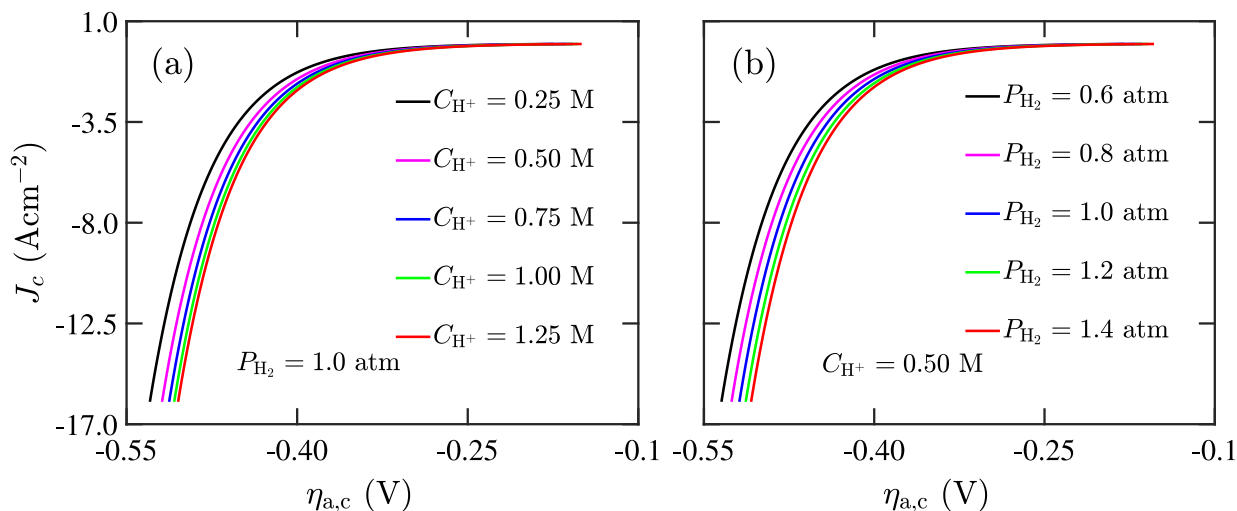


Fig. 8. (a) The effect of C_{H^+} on J_c vs. $\eta_{a,c}$ with $P_{H_2} = 1$ atm, and (b) the effect of P_{H_2} on J_c vs. $\eta_{a,c}$ with $C_{H^+} = 0.25$ M atm for the Ir/Ni(111) electrode, when $\theta_{sc} = 1$ ML.

References

- [1] Bilgen S. Structure and environmental impact of global energy consumption. *Renew Sustain Energy Rev* 2014;38:890–902.
- [2] Bilgen S. Calculation and interpretation of the standard chemical exergies of elements using the chemical reference species. *Acta Phys-Chim Sin* 2009;25(8):1645–9.
- [3] Murthy AP, Theerthagiri J, Madhavan J, Murugan K. Enhancement of hydrogen evolution activities of low-cost transition metal electrocatalysts in near-neutral strongly buffered aerobic media. *Electrochem Commun* 2017;83:6–10.
- [4] Chen Y, Yang K, Jiang B, Li J, Zeng M, Fu L. Emerging two-dimensional nanomaterials for electrochemical hydrogen evolution. *J Mater Chem A* 2017;5(18):8187–208.
- [5] Jiang C, Moniz SJ, Wang A, Zhang T, Tang J. Photoelectrochemical devices for solar water splitting—materials and challenges. *Chem Soc Rev* 2017;46(15):4645–60.
- [6] McKone JR, Marinescu SC, Brunschwig BS, Winkler JR, Gray HB. Earth-abundant hydrogen evolution electrocatalysts. *Chem Sci* 2014;5(3):865–78.
- [7] Murthy AP, Theerthagiri J, Madhavan J. Insights on tafel constant in the analysis of hydrogen evolution reaction. *J Phys Chem C* 2018;122(42):23943–9.
- [8] Yusaf T, Laimon M, Alrefae W, Kadirgama K, Dhahad HA, Ramasamy D, et al. Hydrogen energy demand growth prediction and assessment (2021–2050) using a system thinking and system dynamics approach. *Appl Sci* 2022;12(2):781.
- [9] Du J, Wang L, Bai L, Dang S, Su L, Qin X, et al. Datura-like Ni-HG-rGO as highly efficient electrocatalyst for hydrogen evolution reaction in alkaline conditions. *J Colloid Interface Sci* 2019;535:75–83.
- [10] Jin H, Liu X, Chen S, Vasileff A, Li L, Jiao Y, et al. Heteroatom-doped transition metal electrocatalysts for hydrogen evolution reaction. *ACS Energy Lett* 2019;4(4):805–10.
- [11] Hsieh C-T, Huang C-L, Chen Y-A, Lu S-Y. NiFeMo alloy inverse-opals on Ni foam as outstanding bifunctional catalysts for electrolytic water splitting of ultra-low cell voltages at high current densities. *Appl Catal B* 2020;267:118376.
- [12] Ong W-J, Tan L-L, Ng YH, Yong S-T, Chai S-P. Graphitic carbon nitride ($g\text{-C}_3\text{N}_4$)-based photocatalysts for artificial photosynthesis and environmental remediation: are we a step closer to achieving sustainability? *Chem Rev* 2016;116(12):7159–329.
- [13] Putri LK, Tan L-L, Ong W-J, Chang WS, Chai S-P. Graphene oxide: exploiting its unique properties toward visible-light-driven photocatalysis. *Appl Mater Today* 2016;4:9–16.
- [14] Vesborg PC, Seger B, Chorkendorff I. Recent development in hydrogen evolution reaction catalysts and their practical implementation. *J Phys Chem Lett* 2015;6(6):951–7.
- [15] Wang J, Cui W, Liu Q, Xing Z, Asiri AM, Sun X. Recent progress in cobalt-based heterogeneous catalysts for electrochemical water splitting. *Adv Mater* 2016;28(2):215–30.
- [16] Zeng M, Li Y. Recent advances in heterogeneous electrocatalysts for the hydrogen evolution reaction. *J Mater Chem A* 2015;3(29):14942–62.
- [17] Wang S, Lu A, Zhong C-J. Hydrogen production from water electrolysis: role of catalysts. *Nano Convergence* 2021;8:1–23.
- [18] Zhou W, Jia J, Lu J, Yang L, Hou D, Li G, et al. Recent developments of carbon-based electrocatalysts for hydrogen evolution reaction. *Nano Energy* 2016;28:29–43.
- [19] Sheng W, Myint M, Chen JG, Yan Y. Correlating the hydrogen evolution reaction activity in alkaline electrolytes with the hydrogen binding energy on monometallic surfaces. *Energy Environ Sci* 2013;6(5):1509–12.
- [20] Trasatti S. Work function, electronegativity, and electrochemical behaviour of metals: III. Electrolytic hydrogen evolution in acid solutions. *J Electroanal Chem Interfacial Electrochem* 1972;39(1):163–84.
- [21] Yang TT, Patil RB, McKone JR, Saldi WA. Revisiting trends in the exchange current for hydrogen evolution. *Catal Sci Technol* 2021;11(20):6832–8.
- [22] Marković N, Grgr B, Ross PN. Temperature-dependent hydrogen electrochemistry on platinum low-index single-crystal surfaces in acid solutions. *J Phys Chem B* 1997;101(27):5405–13.
- [23] Zheng J, Sheng W, Zhuang Z, Xu B, Yan Y. Universal dependence of hydrogen oxidation and evolution reaction activity of platinum-group metals on pH and hydrogen binding energy. *Sci Adv* 2016;2(3):e1501602.
- [24] Durst J, Simon C, Hasché F, Gasteiger HA. Hydrogen oxidation and evolution reaction kinetics on carbon supported Pt, Ir, Rh, and Pd electrocatalysts in acidic media. *J Electrochem Soc* 2014;162(1):F190.
- [25] Xu W, Zhu S, Liang Y, Cui Z, Yang X, Inoue A, et al. A highly efficient electrocatalyst based on amorphous Pd–Cu–S material for hydrogen evolution reaction. *J Mater Chem A* 2017;5(35):18793–800.
- [26] Safavi A, Kazemi SH, Kazemi H. Electrocatalytic behaviors of silver–palladium nanoalloys modified carbon ionic liquid electrode towards hydrogen evolution reaction. *Fuel* 2014;118:156–62.
- [27] Kuhn A, Wright P. The cathodic evolution of hydrogen on ruthenium and osmium electrodes. *J Electroanal Chem Interfacial Electrochem* 1970;27(2):319–23.
- [28] Pentland N, Bockris J, Sheldon E. Hydrogen evolution reaction on copper, gold, molybdenum, palladium, rhodium, and iron: mechanism and measurement technique under high purity conditions. *J Electrochem Soc* 1957;104(3):182.
- [29] Wu Y, Li W, Long X, Wu F, Chen H, Yan J, et al. Effect of bismuth on hydrogen evolution reaction on lead in sulfuric acid solution. *J Power Sources* 2005;144(2):338–45.
- [30] Liu Y, Xu X, Sadd M, Kapitanova OO, Krivchenko VA, Ban J, et al. Insight into the critical role of exchange current density on electrodeposition behavior of lithium metal. *Adv Sci* 2021;8(5):2003301.
- [31] Nørskov JK, Bligaard T, Logadottir A, Kitchin J, Chen JG, Pandelov S, et al. Trends in the exchange current for hydrogen evolution. *J Electrochem Soc* 2005;152(3):J23.
- [32] Dresselhaus MS, Thomas I. Alternative energy technologies. *Nature* 2001;414(6861):332–7.
- [33] Bard AJ, Fox MA. Artificial photosynthesis: solar splitting of water to hydrogen and oxygen. *Acc Chem Res* 1995;28(3):141–5.
- [34] Ma L, Hu Y, Chen R, Zhu G, Chen T, Lv H, et al. Self-assembled ultrathin NiCo_2S_4 nanoflakes grown on Ni foam as high-performance flexible electrodes for hydrogen evolution reaction in alkaline solution. *Nano Energy* 2016;24:139–47.
- [35] Theerthagiri J, Lee SJ, Murthy AP, Madhavan J, Choi MY. Fundamental aspects and recent advances in transition metal nitrides as electrocatalysts for hydrogen evolution reaction: A review. *Curr Opin Solid State Mater Sci* 2020;24(1):100805.
- [36] Zheng X, Xu J, Yan K, Wang H, Wang Z, Yang S. Space-confined growth of MoS_2 nanosheets within graphite: the layered hybrid of MoS_2 and graphene as an active catalyst for hydrogen evolution reaction. *Chem Mater* 2014;26(7):2344–53.
- [37] Zhang Z, Chen K, Zhao Q, Huang M, Ouyang X. Electrocatalytic and photocatalytic performance of noble metal doped monolayer MoS_2 in the hydrogen evolution reaction: a first principles study. *Nano Mater Sci* 2021;3(1):89–94.

- [38] Wang P, Zhang X, Zhang J, Wan S, Guo S, Lu G, et al. Precise tuning in platinum-nickel/nickel sulfide interface nanowires for synergistic hydrogen evolution catalysis. *Nat Commun* 2017;8(1):14580.
- [39] Tiwari JN, Sultan S, Myung CW, Yoon T, Li N, Ha M, et al. Multicomponent electrocatalyst with ultralow Pt loading and high hydrogen evolution activity. *Nat Energy* 2018;3(9):773–82.
- [40] Xiong K, Li L, Zhang L, Ding W, Peng L, Wang Y, et al. Ni-doped Mo₂C nanowires supported on Ni foam as a binder-free electrode for enhancing the hydrogen evolution performance. *J Mater Chem A* 2015;3(5):1863–7.
- [41] Pašti I, Mentus S. Electronic properties of the Pt_xMe_{1-x}/Pt (1 1 1) (Me=Au, Bi, In, Pb, Pd, Sn and Cu) surface alloys: DFT study. *Mater Chem Phys* 2009;116(1):94–101.
- [42] Li C, Baek J-B. Recent advances in noble metal (Pt, Ru, and Ir)-based electrocatalysts for efficient hydrogen evolution reaction. *ACS Omega* 2019;5(1):31–40.
- [43] Elnabawy AO, Herron JA, Liang Z, Adzic RR, Mavrikakis M. Formic acid electrooxidation on Pt or Pd monolayer on transition-metal single crystals: A first-principles structure sensitivity analysis. *ACS Catal* 2021;11(9):5294–309.
- [44] Madey TE, Song K-J, Dong C-Z, Demmin RA. The stability of ultrathin metal films on W (110) and W (111). *Surf Sci* 1991;247(2–3):175–87.
- [45] Schröder U, Linke R, Boo J-H, Wandelt K. Growth and characterization of ultrathin Pt films on Cu (111). *Surf Sci* 1996;357:873–8.
- [46] Bai J, Xu G-R, Xing S-H, Zeng J-H, Jiang J-X, Chen Y. Hydrothermal synthesis and catalytic application of ultrathin rhodium nanosheet nanoassemblies. *ACS Appl Mater Interfaces* 2016;8(49):33635–41.
- [47] Wang T, Tao L, Zhu X, Chen C, Chen W, Du S, et al. Combined anodic and cathodic hydrogen production from aldehyde oxidation and hydrogen evolution reaction. *Nat Catal* 2022;5(1):66–73.
- [48] Kadier A, Simayi Y, Kalil MS, Abdeshahian P, Hamid AA. A review of the substrates used in microbial electrolysis cells (MECs) for producing sustainable and clean hydrogen gas. *Renew Energy* 2014;71:466–72.
- [49] Kucernak AR, Zalitis C. General models for the electrochemical hydrogen oxidation and hydrogen evolution reactions: theoretical derivation and experimental results under near mass-transport free conditions. *J Phys Chem C* 2016;120(20):10721–45.
- [50] Shinagawa T, Garcia-Esparza AT, Takanabe K. Insight on Tafel slopes from a microkinetic analysis of aqueous electrocatalysis for energy conversion. *Sci Rep* 2015;5(1):1–21.
- [51] Ma Y-Y, Lang Z-L, Yan L-K, Wang Y-H, Tan H-Q, Feng K, et al. Highly efficient hydrogen evolution triggered by a multi-interfacial Ni₂WC hybrid electrocatalyst. *Energy Environ Sci* 2018;11(8):2114–23.
- [52] Langmuir I. The adsorption of gases on plane surfaces of glass, mica and platinum. *J Am Chem Soc* 1918;40(9):1361–403.
- [53] Chase MW, (US) NIST. NIST-JANAF thermochemical tables, vol. 9, American Chemical Society Washington, DC; 1998.
- [54] Ferreira A, Gonzalez E, Ticianelli E, Avaca LA, Matvienko B. The effect of temperature on the water electrolysis reactions on nickel and nickel-based codeposits. *J Appl Electrochem* 1988;18(6):894–8.
- [55] Kim H, Macdonald DD. Measurement of steady-state hydrogen electrode reactions on Alloys 600 and 690 tubes. *Corros Sci* 2010;52(4):1139–45.
- [56] Davydov A, Rybalka KV, Beketaeva LA, Engelhardt GR, Jayaweera P, Macdonald DD. The kinetics of hydrogen evolution and oxygen reduction on Alloy 22. *Corros Sci* 2005;47(1):195–215.
- [57] Sharifi-Asl S, Macdonald DD. Investigation of the kinetics and mechanism of the hydrogen evolution reaction on copper. *J Electrochem Soc* 2013;160(6):H382.
- [58] Conway B, Tilak B. Interfacial processes involving electrocatalytic evolution and oxidation of H₂, and the role of chemisorbed H. *Electrochim Acta* 2002;47(22–23):3571–94.
- [59] Hiromoto S, Tsai A-P, Sumita M, Hanawa T. Effect of pH on the polarization behavior of Zr₆₃Al_{7.5}Ni₁₀Cu_{17.5} amorphous alloy in a phosphate-buffered solution. *Corros Sci* 2000;42(12):2193–200.
- [60] Schmid A, Fleig J. The current-voltage characteristics and partial pressure dependence of defect controlled electrochemical reactions on mixed conducting oxides. *J Electrochem Soc* 2019;166(12):F831.
- [61] Barbir F. PEM fuel cells: theory and practice. Academic Press; 2012.
- [62] Giannozzi P, Baroni S, Bonini N, Calandra M, Car R, Cavazzoni C, et al. QUANTUM ESPRESSO: a modular and open-source software project for quantum simulations of materials. *J Phys: Condens Matter* 2009;21(39):395502.
- [63] Giannozzi P, Andreussi O, Brumme T, Bunau O, Nardelli MB, Calandra M, et al. Advanced capabilities for materials modelling with quantum ESPRESSO. *J Phys Condens Matter* 2017;29(46):465901.
- [64] Monkhorst HJ, Pack JD. Special points for Brillouin-zone integrations. *Phys Rev B* 1976;13(12):5188.
- [65] Conway B, Jerkiewicz G. Relation of energies and coverages of underpotential and overpotential deposited H at Pt and other metals to the ‘volcano curve’ for cathodic H₂ evolution kinetics. *Electrochim Acta* 2000;45(25–26):4075–83.
- [66] Mamun AA, Billah A, Talukder MA. Effects of activation overpotential in photoelectrochemical cells considering electrical and optical configurations. *Heliyon* 2023;9(6).
- [67] Akbari E, Jahanbin K, Afroozeh A, Yupapin P, Buntat Z. Brief review of monolayer molybdenum disulfide application in gas sensor. *Physica B* 2018;545:510–8.
- [68] Dong H, Hou T, Lee S-T, Li Y. New Ti-decorated B40 fullerene as a promising hydrogen storage material. *Sci Rep* 2015;5(1):9952.
- [69] Pašti IA, Gavrilov NM, Mentus SV. Hydrogen adsorption on palladium and platinum overlayers: DFT study. *Adv Phys Chem* 2011.
- [70] Zhou KL, Wang Z, Han CB, Ke X, Wang C, Jin Y, et al. Platinum single-atom catalyst coupled with transition metal/metal oxide heterostructure for accelerating alkaline hydrogen evolution reaction. *Nature Commun* 2021;12(1):3783.
- [71] Lv F, Feng J, Wang K, Dou Z, Zhang W, Zhou J, et al. Iridium-tungsten alloy nanodendrites as pH-universal water-splitting electrocatalysts. *ACS Cent Sci* 2018;4(9):1244–52.
- [72] Li F, Han G-F, Noh H-J, Jeon J-P, Ahmad I, Chen S, et al. Balancing hydrogen adsorption/desorption by orbital modulation for efficient hydrogen evolution catalysis. *Nat Commun* 2019;10(1):4060.
- [73] Raveendran A, Chandran M, Dhanusuraman R. A comprehensive review on the electrochemical parameters and recent material development of electrochemical water splitting electrocatalysts. *RSC Adv* 2023;13(6):3843–76.
- [74] Tan Y, Xie R, Zhao S, Lu X, Liu L, Zhao F, et al. Facile fabrication of robust hydrogen evolution electrodes under high current densities via Pt@ Cu interactions. *Adv Funct Mater* 2021;31(45):2105579.